On the Mechanism of the Metallo-β-lactamase from *Bacteroides fragilis*[†]

Zhigang Wang, Walter Fast, and Stephen J. Benkovic*

Department of Chemistry, The Pennsylvania State University, 152 Davey Laboratory, University Park, Pennsylvania 16802

Received February 12, 1999; Revised Manuscript Received May 28, 1999

ABSTRACT: The catalytic mechanism of metallo-β-lactamase from *Bacteroides fragilis*, a dinuclear Zn(II)-containing enzyme responsible for multiple antibiotic resistance, has been investigated by using nitrocefin as a substrate. Rapid-scanning and single-wavelength stopped-flow studies revealed the accumulation during turnover of an enzyme-bound intermediate with intense absorbance at 665 nm (ϵ = 30 000 M^{-1} cm^{-1}). The proposed minimum kinetic mechanism for the *B. fragilis* metallo-β-lactamase-catalyzed nitrocefin hydrolysis [Wang, Z., and Benkovic, S. J. (1998) *J. Biol. Chem. 273*, 22402−22408] was confirmed, and more accurate kinetic parameters were obtained from computer simulations and fitting. The intermediate was shown to be a novel anionic species bound to the enzyme through a Zn−acyl linkage and contains a negatively charged nitrogen leaving group. This is the first time such an intermediate was observed in the catalytic cycle of a Zn(II)-containing hydrolase and is evidence for a unique β-lactam hydrolysis mechanism in which the amine can leave as an anion; prior protonation is not required. The electrostatic interaction between the negatively charged intermediate and the positively charged dinuclear Zn(II) center of the enzyme is important for stabilization of the intermediate. The catalytic reaction was accelerated in the presence of exogenous nucleophiles or anions, and neither the product nor the enzyme was modified during turnover, indicating that a Zn-bound hydroxide (rather than Asp-103) is the active site nucleophile. On the basis of all the information on hand, a catalytic mechanism of the *B. fragilis* metallo-β-lactamase is proposed.

β-Lactamases are diverse enzymes produced by some bacterial strains to subvert the lethal action of β-lactam antibiotics through hydrolysis of the β-lactam C−N bond (*1*). The emergence of β-lactamase-mediated antibiotic resistance comprises a serious and increasing problem to human health (*2*, *3*). So far, more than 200 β-lactamases have been identified. They are classified into four structural classes (A−D) based on their primary structures (*4*) or into four functional groups (1−4) based on their functional characteristics and inhibitor profiles (*5*). Class A, C, and D or group 1, 2, and 4 β-lactamases use the hydroxyl group of an active site serine as a nucleophile to attack the carbonyl group of a β-lactam ring followed by the transient formation of an acyl−enzyme intermediate (*1*, *4*, *5*). Mechanism-based inhibitors have been developed to overcome resistance caused by many of the serine β-lactamases (*1*, *4*, *5*). However, there is no clinically useful inhibitor for class B (group 3) enzymes, metallo-β-lactamases that require Zn(II) for their activity and hydrolyze a broad spectrum of β-lactam antibiotics, including carbapenems and other potent mechanism-based inactivators developed for the serine enzymes (*6*). Although only about 20 metallo-β-lactamases have been reported to date, the fact that they are found in a number of human pathogens, including *Aeromonas*, *Bacteroides*, *Chryseobacterium*, *Klebsiella*, *Pseudomonas* and/or *Stenotrophomonas*, and *Serratia* (*7*−*13*), and that some of the genes can be horizontally transferred to obnoxious species (*9*, *11*, *13*) makes them an even more dangerous threat to human health.

Much of the research on metallo-β-lactamases has been focused on their identification, purification, and substrate specificity. So far, more than a dozen genes encoding metallo-β-lactamases have been sequenced (*10*). Besides sharing some conserved motifs, members of the metallo-β-lactamase family exhibit rather large sequence diversity (*1*, *10*, *14*). On the basis of the patterns of sequence similarity, metallo-β-lactamases can be further divided into three subclasses, i.e., B1−B3 (*10*). Class B1 (found in *Bacillus cereus*, *Bacteroides fragilis*, *Serratia marcescens*, *Pseudomonas aeruginosa*, *Klebsiella pneumoniae*, *Pseudomonas putida*, *Alcaligenes xyloxidans*, and *Chryseobacterium meningosepticum*) and class B3 (from *Stenotrophomonas maltophilia*) metallo-β-lactamases can hydrolyze a very broad spectrum of substrates, including penicillins, cephalosporins, and carbapenems (*7*, *15*−*17*), while class B2 enzymes (from *Aeromonas hydrophila*, *Aeromonas veronii*, and *Buckholderia cepacia*) have very narrow substrate profiles, hydrolyzing carbapenems preferentially (*7*, *18*, *19*). Alternatively, Rasmussen and Bush classified the class B/group 3 β-lactamases into three subgroups based on their substrate specificity (*7*). The Rasmussen/Bush group 3a metallo-β-lactamases comprises the class B1 and B3 enzymes, whereas group 3b is the same as class B2 (*7*). Group 3c contains only the metallo-β-lactamase from *Legionella gormanii* which catalyzes the extremely rapid hydrolysis of ampicillin and, especially, cephoridine (*20*). Group 3a metallo-β-lactamases require two Zn(II) ions per monomer for maximal

[†] This work was supported in part by a National Institutes of Health grant (GM 56879-01) to S.J.B. Z.W. was the recipient of a National Institutes of Health postdoctoral fellowship (GM 18061).

* To whom correspondence should be addressed: Department of Chemistry, The Pennsylvania State University, 152 Davey Laboratory, University Park, PA 16802. Phone: (814) 865-2882. Fax: (814) 865-2973. E-mail: sjb1@psu.edu.

10.1021/bi990356r CCC: $18.00
Published on Web 07/13/1999

Scheme 1

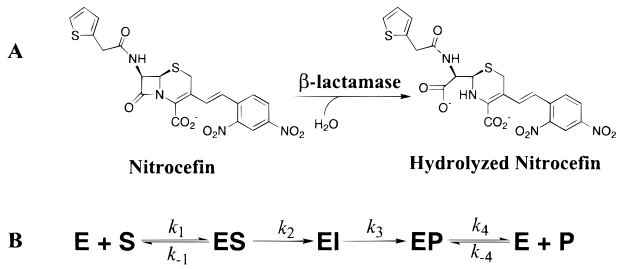

enzymatic activities, but the Zn(II) binding affinities are different from enzyme to enzyme (*21*−*24*). Group 3b enzymes need only one Zn(II) for full activity and are inhibited by the addition of a second Zn(II) ion (*25*). The structural and mechanistic heterogeneity among metallo-β-lactamases make the antibiotic resistance mediated by them even more difficult to combat.

Recently, detailed structural information about the group 3a metallo-β-lactamases emerged with the reports of high-resolution crystal structures of enzymes from *B. cereus* (*26*−*28*), *B. fragilis* (*29*, *30*), and *S. maltophilia* (*31*). The overall three-dimensional structures of the three metallo-β-lactamases are quite similar (*31*). They all exhibit the unique $\alpha\beta/\beta\alpha$ folds and employ a dinuclear Zn(II) center as their active site with most of the Zn(II) ligands conserved (*31*). These structural similarities dictate their similar enzymatic properties. In addition, the substrate binding pocket in each enzyme can accommodate a variety of β-lactam molecules, providing the structural basis for the broad substrate specificity of these enzymes (*31*). It is the subtle differences in the Zn(II) centers and the substrate binding sites that determine their catalytic efficiencies toward various substrates.

The differences among metallo-β-lactamases from different sources suggest that a single class of inhibitors may not be effective against the whole family. Understanding and exploiting the structural and mechanistic features found in metallo-β-lactamases from different sources is an important first step toward the development of new antibiotics for combatting the emerging antibiotic resistance spread by metallo-β-lactamases. However, mechanistic studies have only been carried out with the one-Zn(II) metallo-β-lactamase from *B. cereus* (*32*−*35*). How the dinuclear Zn(II) center catalyzes the hydrolysis of β-lactam rings remains to be determined. In our previous work (*22*), by using nitrocefin as a substrate, we were able to establish the minimal kinetic mechanism (Scheme 1) of the dinuclear Zn(II)-containing metallo-β-lactamase from *B. fragilis*, one of the more important anaerobic pathogens commonly found in suppurative and/or surgical infections (*36*−*38*). Preliminary results showing the accumulation of an enzyme-bound intermediate during the *B. fragilis* catalytic cycle were also obtained by using a rapid-scanning stopped-flow technique (*39*). In this work, rapid-scanning and single-wavelength stopped-flow studies were carried out to further assess the kinetic mechanism of this enzyme. The identities of the nucleophile attacking the C−N bond of the β-lactam ring and the observed enzyme-bound intermediate have also been established. A catalytic mechanism for the *B. fragilis* metallo-β-lactamase-catalyzed nitrocefin hydrolysis is proposed.

EXPERIMENTAL PROCEDURES

Materials. The *B. fragilis* metallo-β-lactamase was purified according to the procedures described previously and subjected to 72 h of dialysis against metal-free 50 mM HEPES buffer (pH 7.6) at 4 °C to remove adventitious metal ions (*22*). The purity and Zn(II) content of each protein preparation were ascertained by SDS−PAGE[1] and flame mode atomic absorption analysis by using a Perkin-Elmer 730 atomic absorption spectrophotometer at the Pennsylvania State Materials Characterization Laboratory, respectively. The protein concentration was determined by using an ϵ_{280} of 39 000 M^{-1} cm^{-1} (*22*). Co(II)-substituted *B. fragilis* metallo-β-lactamase was prepared as described previously (*22*). Nitrocefin was purchased from Becton Dickinson. All other chemicals were either analytical reagents or molecular biology grade.

Stopped-Flow Kinetic Studies of the B. fragilis Metallo-β-lactamase. All the stopped-flow experiments were carried out in 1× MTEN buffer (50 mM Mes, 25 mM Tris, 25 mM ethanolamine, and 100 mM NaCl) at the specified pH or pD and 25 °C. In a typical experiment, a solution of *B. fragilis* metallo-β-lactamase was rapidly mixed with a nitrocefin solution in an Applied Photophysics SX.18MV stopped-flow spectrometer. Absorbance changes that occurred during the reaction were monitored with either an Applied Photophysics PD.1 photodiode array detector (2.56 ms scan intervals) over the wavelength range of 310−725 nm or an absorbance photomultiplier at 390, 490, and 665 nm. Data from at least three reproducible experiments were collected, averaged, and corrected for the instrument dead time (1.5 ms). The rapid-scanning stopped-flow data were analyzed globally (*40*) by using the Applied Photophysics !ProK software to converge the correct kinetic scheme, rate constants, and the absorbance spectrum of the intermediate. The molar extinction coefficients of nitrocefin (ϵ_{390} = 14 920 M^{-1} cm^{-1}, ϵ_{490} = 1520 M^{-1} cm^{-1}), hydrolyzed nitrocefin (ϵ_{390} = 5840 M^{-1} cm^{-1}, ϵ_{490} = 17 200 M^{-1} cm^{-1}), and the intermediate (derived from the absorbance spectrum generated from the global analysis) were used to convert the single-wavelength stopped-flow absorbance data to concentration data representing the substrate, intermediate, and product and to correct for overlapping absorption profiles. The concentration data sets were simulated with the program Kinsim using an appropriate kinetic mechanism (C. Frieden and B. Barshop, Washington University, St. Louis, MO) (*41*, *42*). Acceptable ranges of rate constants were judged by either Fitsim fits, Kinsim simulations, or both.

Preparation and Deprotonation of Hydrolyzed Nitrocefin. Hydrolyzed nitrocefin was produced by reacting nitrocefin (250 μM) with the *B. fragilis* metallo-β-lactamase (25 nM) in 1× MTEN buffer (pH 7.0, 100 μL). After the reaction was complete, the pH of the reaction mixture was adjusted to ca. 4.0 with 1 M HCl and the mixture extracted twice with 400 μL of ethyl acetate. The organic solvent was then

[1] Abbreviations: ϵ, extinction coefficient; ESI, electrospray ionization; HEPES, *N*-(2-hydroxyethyl)piperazine-*N*′-2-ethanesulfonic acid; MALDI, matrix-assisted laser desorption ionization; Mes, 2-(*N*-morpholino)ethanesulfonic acid; MS, mass spectrometry; *m*/*z*, mass-to-charge ratio; SDS−PAGE, sodium dodecyl sulfate−polyacrylamide gel electrophoresis; THF, tetrahydrofuran; Tris, tris(hydroxymethyl)-aminomethane; UV−vis, ultraviolet−visible; *v*, steady-state rate of product formation.

evaporated with an argon flow to yield the dry product. The product was ascertained to be hydrolyzed nitrocefin by its UV−vis spectrum and by ESI-MS analysis on a PerSpective Biosystems Mariner mass spectrometer at the Pennsylvania State Mass Spectrometry Center.

Deprotonation of hydrolyzed nitrocefin was monitored spectroscopically at 25 °C on a Varian Cary-1 UV−vis spectrophotometer. Briefly, small aliquots (less than 2% of the total volume) of a strong base (butyllithium [$CH_3(CH_2)_3$-Li], phenyllithium (C_6H_5Li), lithium diisopropylamide {[$(CH_3)_2CH]_2NLi$}, or potassium *tert*-butoxide [$(CH_3)_3COK$]) were added to 1.0 mL of the hydrolyzed nitrocefin solution (in THF) in a quartz cuvette. The UV−vis spectrum of the mixture was monitored after each addition until the spectral change was complete. To reprotonate and recover hydrolyzed nitrocefin, small aliquots of Milli Q water (Millipore) were added to the mixture until the original color reappeared. After evaporation of all the THF solvent from the mixture, two changes of 400 μL of ethyl acetate were used to extract the recovered hydrolyzed nitrocefin. The dry product was obtained by removing ethyl acetate with an argon flow and was subjected to ESI-MS analysis.

Enzyme Assays in the Presence of Nucleophiles or Anions. The steady-state rates of *B. fragilis* metallo-β-lactamase-catalyzed nitrocefin hydrolysis in the presence of α-effect nucleophiles (hydroxylamine and methoxylamine) and various anions (sodium salts of fluoride, acetate, fluoroacetate, azide, cyanate, thiocyanate, and hydrosulfide) were determined at 25 °C in 1× MTEN buffer (pH 7.0) containing the corresponding nucleophile or anion. In each reaction, 1.15 nM enzyme and a saturating amount of substrate (100 μM) were mixed and absorbance changes at 490 nm monitored for product formation (*22*). The obtained rates were then corrected for the background hydrolysis of nitrocefin caused by the corresponding nucleophiles and anions. Ionic strength effects on the enzyme activity were ascertained by carrying out the assay in the presence of sodium chloride at concentrations of up to 2 M. To determine whether the enzyme loses its activity after multiple turnovers in the presence of nucleophiles and anions, 25 nM *B. fragilis* metallo-β-lactamase was first used to hydrolyze 250 μM nitrocefin completely at 25 °C in 1× MTEN buffer (pH 7.0) containing the corresponding nucleophile or anion (10 000 turnovers). The reaction mixture was then assayed for β-lactamase activity, and the results were compared with that of a control incubation lacking the exogenous nucleophile or anion. Single-wavelength and rapid-scanning stopped-flow experiments on nitrocefin hydrolysis catalyzed by the *B. fragilis* metallo-β-lactamase in the presence of nucleophiles and anions were carried out according to the procedures described previously except that the corresponding nucleophiles and anions (2 × concentration) were added in the enzyme solution.

Mass Spectrometric Analysis of the Hydrolytic Products and Enzymes after Turnovers. The products of nitrocefin hydrolysis in the presence of nucleophiles and some of the anions were obtained according to the same procedures employed for the hydrolyzed nitrocefin preparation except that the nucleophiles and anions were present in the reaction buffer. The molecular mass of each product was determined by ESI-MS analysis. To prepare protein samples for mass spectrometric analysis, reactions of 300 μM nitrocefin with 3 μM enzyme were carried out in 300 μL of 1× MTEN buffer (pH 7.0) containing the desired nucleophile or anion. The reaction mixtures were then passed through Sephadex G-25 (Amersham Pharmacia) spin columns equilibrated with Milli Q water at 4 °C to remove the product and salts. The obtained salt-free protein solutions were concentrated with Centricon-10 concentrators (Amicon). Mass spectra of the protein samples were acquired on a PerSpective Biosystems Voyager-DE STR time-of-flight (TOF) mass spectrometer by MALDI with the 337 nm line of a nitrogen laser at the Pennsylvania State Mass Spectrometry Center. The matrix solution for MALDI analysis was saturated sinapinic acid in a solvent system of acetonitrile/water. Bovine serum albumin (BSA) was used as the *m*/*z* calibrator.

RESULTS

Kinetic Analysis of the B. fragilis Metallo-β-lactamase. Nitrocefin, (6*R*,7*R*)-3-[(2,4-dinitro)styryl]-8-oxo-7-[(2-thienylacetyl)amino]-5-thia-1-azabicyclo[4.2.0]oct-2-ene-2-carboxylic acid, and its hydrolyzed product have very different absorbance spectra (Scheme 1A) (*43*). In our preliminary rapid-scanning stopped-flow studies, the reaction of 5 μM *B. fragilis* metallo-β-lactamase with 10 μM nitrocefin was monitored with a photodiode array detector between 310 and 725 nm over a time period of 100 ms (*39*). In addition to the disappearance of the absorbance band at 390 nm (substrate depletion) and the appearance of the absorbance band at 490 nm (product formation), a new absorbance feature was observed at 665 nm whose intensity increased rapidly and then decreased at a slower rate (*39*). Similar results were also observed when other concentrations of the *B. fragilis* metallo-β-lactamase (2.5 and 10 μM) and nitrocefin (5 and 20 μM) were mixed at pH 7.0 and when various concentrations of enzyme (2.5, 5, and 10 μM) and nitrocefin (5, 10, and 20 μM) were reacted at pH 5.5 and pD 7.0 (data not shown). This is direct proof that an intermediate with strong absorbance at 665 nm accumulates during the reaction, consistent with our previous proposal (*22*). The two binding steps given by the rate constants k_1 and k_{-4} were set to the diffusion-controlled limit (10^8 M^{-1} s^{-1}), and the Michaelis complexes, ES and EP, were assumed to have the same visible absorbance spectra as S and P, respectively. Using these assumptions, global analysis (*40*) of the absorbance changes at all wavelengths extracted the absorption spectrum of the enzyme-bound intermediate (EI) and rate constants for the four-step kinetic mechanism shown in Scheme 1B (*39*). The intermediate has a broad absorbance peak at 665 nm with a molar extinction coefficient of 30 000 M^{-1} cm^{-1} (*39*).

Single-wavelength stopped-flow analyses were carried out at 390, 490, and 665 nm to further characterize the kinetic mechanism. The obtained absorbance data were converted into concentrations by using the method described in Experimental Procedures. Figure 1 displays the three concentration data sets ([S] + [ES], [EI], and [EP] + [P]) from the reaction of 5 μM enzyme with 10 μM nitrocefin at pH 7.0. These data sets were simultaneously simulated using the program Kinsim and Scheme 1B. The simulated curves are shown as solid lines in Figure 1, and the kinetic constants with k_1 and k_{-4} set as diffusion-controlled limits and their estimated uncertainties (see Experimental Procedures) are listed in Table 1. Data from the reaction of 5 μM enzyme

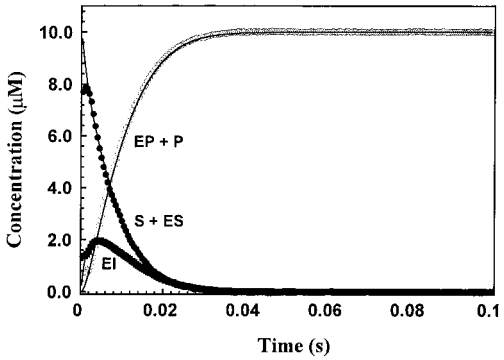

FIGURE 1: Time courses for the *B. fragilis* Zn(II)−β-lactamase-catalyzed hydrolysis of nitrocefin at pH 7.0 and 25 °C. A solution of 20 μM nitrocefin was rapidly mixed with a solution of 10 μM Zn(II)−β-lactamase to initiate the reaction at 25 °C. The intermediate concentration (■) was calculated from the A_{665}−time curve using an ϵ of 30 000 M^{-1} cm^{-1}, while the substrate (●) and product concentrations (○) were calculated from A_{390}−time and A_{490}−time curves with the intermediate, substrate, or product contribution to the absorbance taken into account. The solid lines are simulated curves using the program Kinsim with the kinetic mechanism shown in Scheme 1B and rate constants summarized in Table 1. Data obtained during the instrument's dead time (1.5 ms, represented by the lags in the data sets) were ignored during fitting.

Table 1: Simulated Kinetic Constants of the *B. fragilis* Metallo-β-lactamase-Catalyzed Nitrocefin Hydrolysis at 25 °C

	pH 7.0	pH 5.5	pD 7.0
k_1 (M^{-1} s^{-1})	1×10^8	1×10^8	1×10^8
k_{-1} (s^{-1})	4500 ± 700	1250 ± 300	7800 ± 200
k_2 (s^{-1})	3700 ± 500	3700 ± 500	3100 ± 100
k_3 (s^{-1})	349 ± 3	217 ± 10	119 ± 5
k_4 (s^{-1})	$\geq 1 \times 10^4$	$\geq 1 \times 10^4$	$\geq 1 \times 10^4$
k_{-4} (M^{-1} s^{-1})	1×10^8	1×10^8	1×10^8
$k_{cat,calcd}$[a] (s^{-1})	309	203	113
$K_{M,calcd}$[a] (μM)	6.8	2.7	3.9
$k_{cat,exp}$[b] (s^{-1})	226 ± 6	132 ± 7	90 ± 2
$K_{M,exp}$[b] (μM)	7 ± 0.7	2.6 ± 0.4	4.1 ± 0.4

[a] Steady-state parameters were calculated according to the net rate constant method described by Cleland (*44*), i.e., $k_{cat} = k_2k_3k_4/(k_2k_3 + k_2k_4 + k_3k_4)$; $K_M = (k_{-1} + k_2)k_{cat}/k_1k_2$ for Scheme 1B. [b] Data taken from ref *22*.

with 10 μM nitrocefin at pH 5.5 and pD 7.0 were analyzed in the same manner; they were also well-simulated by the same kinetic mechanism (Scheme 1B) with the kinetic parameters listed in Table 1. Although the ranges listed in Table 1 indicate reasonably robust fits, we found that k_{-1} and k_2 could be set over a wider range if varied as a pair. The values that are shown are those obtained by constraining this pair of constants to provide calculated steady-state parameters, k_{cat} and K_M (*44*), consistent with experimentally measured values (Table 1) (*22*). The rate of product release (k_4) can have a value $\geq 10^4$ s^{-1} for acceptable simulations. The new kinetic parameters are similar to those obtained from Kinsim simulations of the single-turnover data in our previous work (*22*) and are also in agreement with the constants obtained by global analysis (*39*). These results confirm that Scheme 1B indeed represents the minimum kinetic mechanism of nitrocefin hydrolysis by *B. fragilis* metallo-β-lactamase and that the breakdown of the enzyme-bound intermediate (EI) is the rate-determining step.

Deprotonation Studies of Hydrolyzed Nitrocefin. The intense absorbance at 665 nm of the enzyme-bound intermediate, a 175 nm red shift from that of hydrolyzed nitrocefin

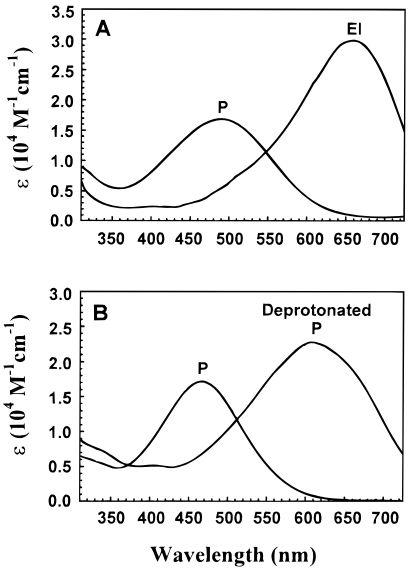

FIGURE 2: Visible spectra of (A) hydrolyzed nitrocefin and the observed enzyme-bound intermediate in 1× MTEN buffer (pH 7.0) and (B) hydrolyzed nitrocefin and its deprotonated product with butyllithium in THF.

(Figure 2A), suggests that it may contain an anionic dihydrothiazine nitrogen (*39*). We attempted to reproduce the spectrum of this proposed intermediate by treating hydrolyzed nitrocefin with strong base and monitoring the spectral changes associated with the deprotonation process. Strong bases may deprotonate more than one center in the hydrolyzed nitrocefin molecule (Scheme 1A), but significant spectral changes are expected to occur only when the nitrogen in the dihydrothiazine ring becomes negatively charged and, in turn, extends the π-electron conjugation.

Hydrolyzed nitrocefin was prepared from the enzymatic reaction as described in Experimental Procedures. In aqueous solution, the purified hydrolyzed nitrocefin exhibited a visible spectrum almost identical to that of the finished reaction mixture of nitrocefin with the enzyme (data not shown). ESI-MS analysis determined the molecular mass of the hydrolyzed nitrocefin to be 534 Da, the value expected after β-lactam hydrolysis. Hydrolyzed nitrocefin exhibited a strong absorbance peak at 469 nm with a molar coefficient of ca. 17 000 M^{-1} cm^{-1} in THF (Figure 2B). When butyllithium [$CH_3(CH_2)_3Li$], a strong, non-nucleophilic base, was added to the above solution, the absorbance band experienced an increase in intensity and red shifted to 612 nm (Figure 2B). The original color could be returned after adding water to the base-treated solution. The recovered compound was found to have the same molecular mass as the starting material as determined by ESI-MS analysis, indicating that the compound remained intact throughout the spectral changes. Similar results were also obtained with other strong, non-nucleophilic bases, including phenyllithium (C_6H_5Li), lithium diisopropylamide {[$(CH_3)_2CH]_2NLi$}, and potassium *tert*-butoxide [$(CH_3)_3COK$] (Table 2). These observations demonstrated that an intense and red-shifted absorbance band similar to the one observed for the enzyme-bound intermediate could be obtained by deprotonating hydrolyzed nitrocefin. Therefore, the enzyme-bound intermediate observed during the catalytic cycle of the *B. fragilis* metallo-β-lactamase is most likely an anionic species containing a negatively

Table 2: Comparison of the Visible Absorbance Features of Hydrolyzed Nitrocefin (P), the Enzyme-Bound Intermediate (EI), and Hydrolyzed Nitrocefin Treated with Different Bases

species	λ (nm)	ν (cm^{-1})	ϵ (M^{-1} cm^{-1})	$\Delta\lambda^a$ (nm)	$\Delta\nu^a$ (cm^{-1})
P in 1× MTEN (pH 7.0)	490	20 408	17 200	−	−
EI in 1× MTEN (pH 7.0)	665	15 308	30 000	175	−5100
P in THF	469	21 322	17 000	−	−
P and $CH_3(CH_2)_3Li$ in THF	612	16 340	23 271	143	−4982
P and C_6H_5Li in THF	610	16 393	31 267	141	−4928
P and $[(CH_3)_2CH]_2NLi$ in THF	622	16 077	23 149	153	−5245
P and $(CH_3)_3COK$ in THF	647	15 456	18 785	178	−5866

[a] Differences between the absorbance features of EI and P in 1× MTEN buffer (pH 7.0) or between the absorbance features of the deprotonated P and P in THF.

Scheme 2: Dinuclear Zn(II) Active Site of the *B. fragilis* Metallo-β-lactamase

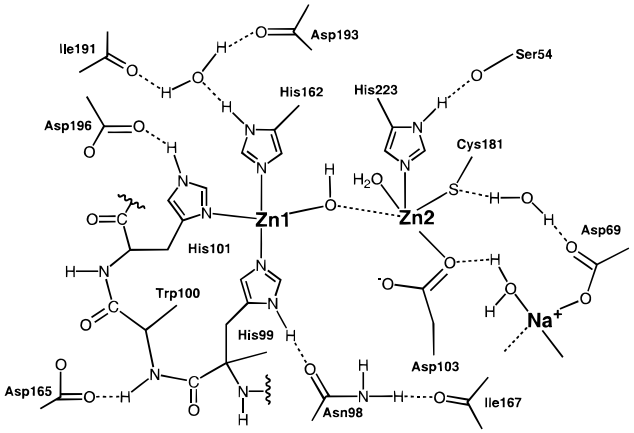

charged nitrogen resulting from fission of the β-lactam C−N bond (*39*).

Effects of Hydroxylamine and Methoxylamine on Metallo-β-lactamase Activity. The enzyme-bound intermediate is presumably formed by nucleophilic attack on the β-lactam carbonyl followed by cleavage of the C−N bond. One possible candidate for the active site nucleophile is the carboxylate of Asp-103, an active site residue conserved in all of the known metallo-β-lactamase sequences (Scheme 2). An Asp-103 attack on the β-lactam carbonyl should generate a mixed anhydride intermediate, the breakdown of which could be accelerated by addition of α-effect nucleophiles such as hydroxylamine and methoxylamine and should result in covalent modification of either the enzyme at Asp-103 or the product (Scheme 3A). In fact, the steady-state rates of *B. fragilis* metallo-β-lactamase-catalyzed nitrocefin hydrolysis were significantly enhanced with the addition of hydroxylamine and methoxylamine in the assay buffer (Figure 3). Similar results were also obtained from stopped-flow experiments (data not shown). In the presence of hydroxylamine or methoxylamine, a transient intermediate with absorbance at 665 nm was observed by rapid-scanning stopped-flow analysis, but the amount of intermediate accumulated was far less than that observed in the reaction without nucleophiles. The single-wavelength stopped-flow data obtained in the presence of hydroxylamine and methoxylamine were very well simulated by Kinsim using Scheme 1B. The data obtained with and without the exogenous nucleophiles were well fit by keeping all of the kinetic parameters the same except for the breakdown rate of the intermediate (k_3) which increased in the presence of hydroxylamine (1250 ± 10 s^{-1}) and methoxylamine (725 ± 6 s^{-1}). These results suggest that exogenous nucleophiles such as hydroxylamine and methoxylamine accelerate the breakdown of the intermediate, as expected for a mixed anhydride mechanism. However, when enzyme aliquots from incubations containing nucleophiles were assayed, their activities were the same as that of the enzyme samples taken from incubations omitting nucleophiles (Table 3), ruling against covalent enzyme modification by hydroxylamine and methoxylamine. Tight, noncovalent interactions with the resting enzyme active site were also not apparent as neither hydroxylamine nor methoxylamine affects the spectrum of the Co(II)-substituted enzyme at the concentrations that were used (data not shown). The hydrolysis products and the enzymes from reactions including hydroxylamine and methoxylamine were isolated and analyzed by ESI-MS and MALDI-MS, respectively; no molecular mass increase was found in either the product or the enzyme for either reaction (Table 3). Therefore, neither the product nor the enzyme was labeled by the nucleophiles during turnover, in contrast to the notion that Asp-103 acts as the nucleophile.

The molecular mass of the enzyme determined from MALDI analyses, 25337−25341 Da, matches well with the expected value for the apoprotein without the N-terminal methionine residue (25 335 Da), suggesting that the active site Zn(II) ions and water were removed by the MALDI process. A small *m*/*z* peak corresponding to a species with a molecular mass of ca. 25 465 Da was also observed in all the protein MALDI-MS spectra. It represents the apoprotein with the first methionine residue (25 466 Da) still attached.

Effects of Anions on the Metallo-β-lactamase Activity. Simple anions, which can also act as Zn(II) ligands, were employed to further explore the interaction between the dinuclear Zn(II) center and the negatively charged intermediate. Results from assays carried out in the presence of sodium chloride (up to 2 M) demonstrated that the enzyme activity is not affected by ionic strength effects (data not shown). However, the steady-state rates of *B. fragilis* metallo-β-lactamase-catalyzed nitrocefin hydrolysis were accelerated by fluoride, acetate, fluoroacetate, and azide (Figure 4). The fact that none of the above anions caused detectable visible spectral changes with the dicobalt-substituted enzyme (data not shown) indicated that they do not strongly interact with the dinuclear metal-binding site of the resting enzyme. Thus, their acceleration on enzyme activity was attributed to their role in promoting the breakdown of the enzyme-bound intermediate to form the product. This argument is supported by the results obtained from the stopped-flow experiments carried out in the presence of these anions (data not shown). In addition, MALDI-MS analysis did not provide evidence for attachment of these anions to side chains of the enzyme.

In contrast to the anions discussed above, the very good Zn(II) ligand, cyanate, did affect the visible spectrum of the Co(II)-substituted *B. fragilis* metallo-β-lactamase (Figure 5), suggesting that cyanate can bind directly to the active site of the resting enzyme. In the presence of lower concentrations of cyanate (<0.25 M), the steady-state rate of *B. fragilis* metallo-β-lactamase-catalyzed nitrocefin hydrolysis was accelerated (Figure 6). However, with high cyanate concentrations (0.25−1.0 M), the hydrolysis rate initially increased significantly followed by enzyme inactivation caused by the

Scheme 3: Two Possible Pathways[a]

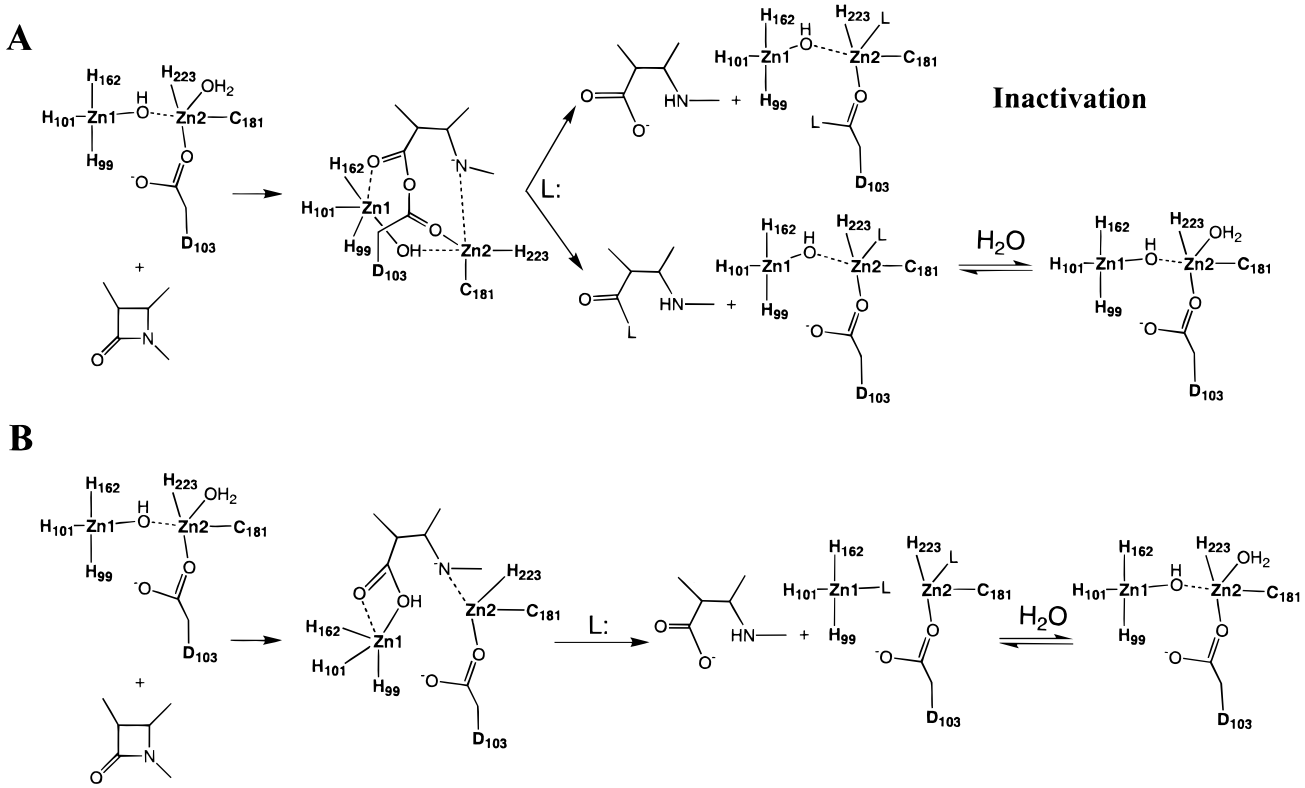

[a] L being a nucleophile or an anion.

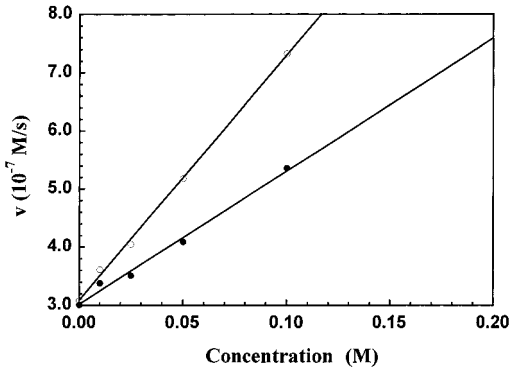

FIGURE 3: Activation of the *B. fragilis* Zn(II)−β-lactamase-catalyzed hydrolysis of nitrocefin by hydroxylamine (○) and methoxylamine (●) at pH 7.0 and 25 °C. In each assay, 1.15 nM enzyme and a saturating amount of substrate (100 μM) were used and the steady-state rate for the product formation was determined as described in Experimental Procedures.

direct binding of the anion to the enzyme active site (Figure 6). Simultaneous Kinsim simulations of the turnover curves from the enzyme-catalyzed nitrocefin hydrolysis in the presence of various amounts of cyanate were only achieved when a kinetic mechanism and rate constants shown in Scheme 4 were employed (Figure 6). Scheme 4 is rather complicated. A number of simpler kinetic schemes, including those in which cyanate only interacts with E, ES, EI, or EP individually or with a subset of bound enzyme forms and schemes in which 1 or 3 equiv of cyanate binds to different bound enzyme forms, were also tested. While all of these schemes can fit a subset of the curves shown in Figure 6, only Scheme 4 allowed simultaneous simulation of all six curves. This mechanism suggests that at least three cyanates

Table 3: Comparison of the Molecular Mass of the Product and the Molecular Mass and Specific Activity of the Enzyme after Multiple Turnovers in the Absence and Presence of Nucleophiles

	molecular mass of the product (Da)	molecular mass of the enzyme (Da)	steady-state rate ($\times 10^{-7}$ M s^{-1})[a]
no nucleophile	534.0	25 337.3	2.61
100 mM NH_2OH	534.2	25 340.9	2.60
100 mM NH_2OCH_3	534.2	25 336.9	2.64

[a] Assay conditions were as follows: $[S]_0 = 100$ μM, and $[E]_0 = 1.15$ nM (the enzyme was taken from the preincubation mixture of 250 μM nitrocefin and 25 nM of enzyme in the presence or absence of the corresponding nucleophile) in 1× MTEN buffer (pH 7.0).

can bind to the enzyme active site; the enzyme is inactivated when the third cyanate binds. The strong zinc ligands, thiocyanate and hydrosulfide, were also tested in this work. The former inhibits the enzyme slightly (Figure 4), while the later removes Zn(II) ions from the enzyme in a time-dependent manner (data not shown).

DISCUSSION

Kinetic Mechanism. By using a rapid-scanning stopped-flow technique, we demonstrated that at room temperature under normal aqueous conditions, a spectral enzyme-bound intermediate accumulates during nitrocefin hydrolysis by the *B. fragilis* metallo-β-lactamase. This observation is direct proof of our previous proposal based on a mass balance deficit obtained from single-wavelength stopped-flow studies under single-turnover conditions (*22*). Results from extensive single-wavelength and rapid-scanning stopped-flow studies confirmed the minimum kinetic mechanism for nitrocefin

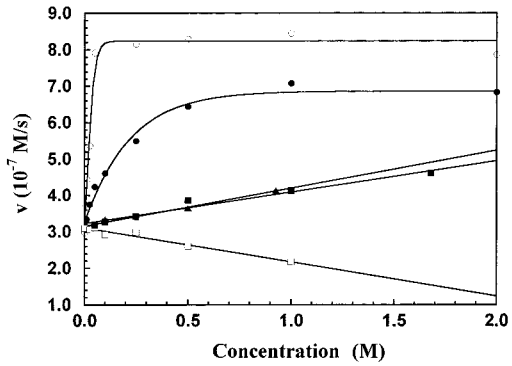

FIGURE 4: Effects of azide (○), acetate (●), fluoroacetate (■), fluoride (▲), and thiocyanate (□) on the steady-state rate of the *B. fragilis* Zn(II)−β-lactamase-catalyzed nitrocefin hydrolysis at pH 7.0 and 25 °C. In each assay, 1.15 nM enzyme and a saturating amount of substrate (100 μM) were used and the steady-state rate for the product formation was determined as described in Experimental Procedures.

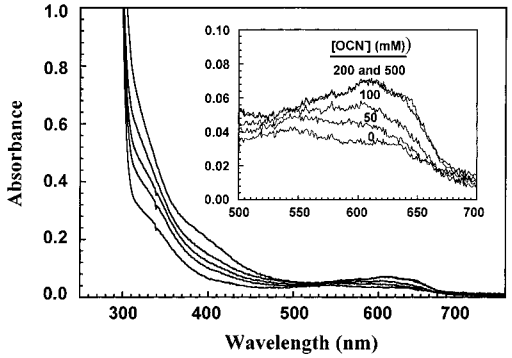

FIGURE 5: Interaction of cyanate with the Co(II)-substituted *B. fragilis* metallo-β-lactamase. The UV−vis spectra of the Co(II) enzyme (140 μM) in the presence of various amounts of cyanate were recorded on an OLIS Cray-14 spectrophotometer at 25 °C.

hydrolysis by the *B. fragilis* metallo-β-lactamase (Scheme 1B). This minimal scheme involves four steps: substrate binding, formation of the intermediate (EI), breakdown of the intermediate to form the product, and product release. The breakdown of the intermediate (k_3) is the rate-limiting step.

With a knowledge of the spectral characteristics of the enzyme-bound intermediate extracted from global analysis, more reliable concentration changes for each species during turnover were derived from the time-dependent absorbance changes. These data, in turn, allowed us to determine more accurate kinetic parameters for each step by using Kinsim and Fitsim (Table 1). The kinetic parameters obtained are similar to those from our previous kinetic studies in which the absorbance of the intermediate at 390 and 490 nm was neglected due to the lack of spectral information (*22*). The assumption that the Michaelis complexes, ES and EP, have the same visible absorbance bands as those of the substrate (S) and product (P), respectively, is likely to be correct as no absorbance features other than those at 390, 490, and 665 nm were observed during the catalytic cycle. The molar extinction coefficient of the enzyme-bound intermediate at 665 nm (30 000 M^{-1} cm^{-1}) is very close to the value obtained for a similar intermediate observed during nitrocefin hydrolysis by the *S. maltophilia* metallo-β-lactamase (32 000 M^{-1} cm^{-1}) by Crowder and co-workers (*45*).

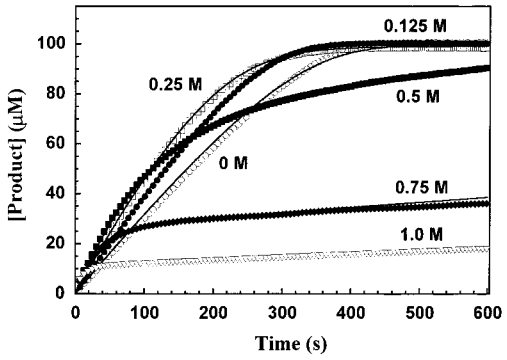

FIGURE 6: Effects of cyanate on the *B. fragilis* Zn(II)−β-lactamase-catalyzed nitrocefin hydrolysis at pH 7.0 and 25 °C. In each assay, 1.15 nM enzyme and a saturating amount of substrate (100 μM) were used. The absorbance change at 490 nm was monitored and then converted into product concentration as described in Experimental Procedures. The data points represent the experimental results, while the solid lines are simulated curves using the program Kinsim with the kinetic mechanism and rate constants shown in Scheme 4. Cyanate concentrations are shown besides each corresponding data point or curve set.

Identity of the Intermediate. The visible absorbance bands of nitrocefin and its hydrolyzed product (390 and 490 nm, respectively) are due to the high degree of conjugation formed by the 2,4-dinitrostyryl substituent in the 3-position, the carboxylate group at the 2-position, and the double bond of the dihydrothiazine ring of these compounds (Scheme 1A). The 100 nm red shift of the absorbance band of the product from that of the substrate is a result β-lactam ring cleavage. However, the 175 nm absorbance red shift of the intermediate from that of the product is far greater than the changes likely caused by the hydrophobic environment of the chromophore upon binding to the enzyme, the planarity of the chromophore, or the positioning of charges near the chromophore (*33*, *46*, *47*). The most likely cause of the red shift is an increase in the extent of conjugation. This shift can be realized if the enzyme-bound intermediate is similar to hydrolyzed nitrocefin, yet the leaving nitrogen atom is not protonated during the cleavage of the C−N bond and remains negatively charged (*39*). We tested this proposal directly by removing the N−H proton of the dihydrothiazine ring of hydrolyzed nitrocefin with strong base to produce a negatively charged species and by monitoring the UV−vis spectrum during the deprotonation. However, our first attempt to deprotonate hydrolyzed nitrocefin with sodium methoxide failed because of rapid degradation of the compound (*39*). To avoid the breakdown of the compound, four non-nucleophilic bases, butyllithium, phenyllithium, lithium diisopropylamide, and potassium *tert*-butoxide, were used in the work presented here. THF was chosen as the solvent because its dielectric constant (7.6 at 20 °C) is close to those of protein active sites and its C−H protons have high pK_a values. Indeed, species with intense, well-red-shifted (>100 nm) absorbance features were obtained after treating hydrolyzed nitrocefin with each of the four bases (Figure 2B and Table 2). The similarity between panels A and B of Figure 2 is striking. In addition, no degradation of hydrolyzed nitrocefin was observed in all four cases, indicating that the color changes are solely due to the reversible deprotonation of the compound. These observations provided direct evidence that the intermediate observed during the *B. fragilis* metallo-β-lactamase-catalyzed nitrocefin hydrolysis is a novel

Scheme 4: Proposed Kinetic Mechanism in the Presence of Cyanate[a]

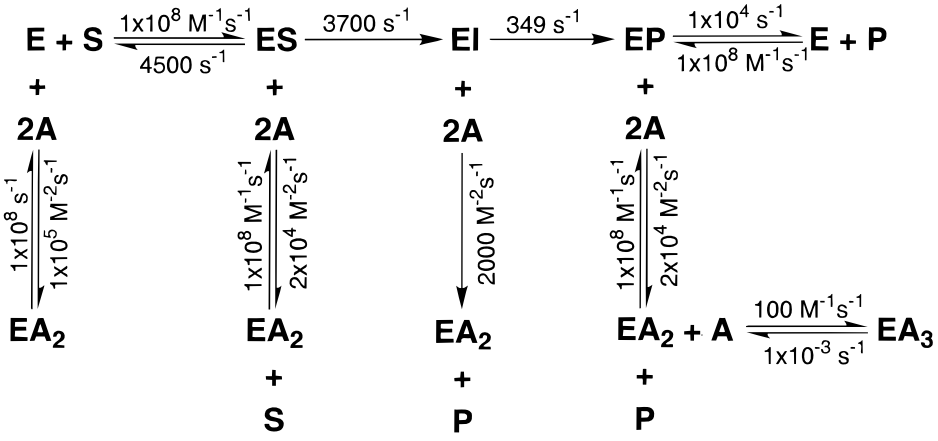

[a] A being cyanate.

anionic species in which the leaving nitrogen is negatively charged upon the cleavage of the β-lactam C−N bond. The small differences between the spectra of deprotonated nitrocefin in THF and the enzyme-bound intermediate may be the result of minor contributions by the enzyme environment. The observation of a hydrogen−deuterium kinetic solvent isotope effect of 2.9 on k_3 is consistent with assigning a protonation event to the decay of EI (Table 1).

Which enzyme group in the active site acts as the nucleophile to attack the carbonyl group of the β-lactam ring, initiating the reaction? Our previous pH dependence studies indicated that the pK_a value of the nucleophile is less than 5.25 (*22*). The apical water molecule bound to the Zn2 may have a decreased pK_a, but is an unlikely candidate because no protein groups, including Asp-103, are appropriately positioned to lower its pK_a value to less than 5.25 (Scheme 2). Therefore, the carboxylate of the conserved Asp-103 and the Zn1 hydroxide are the remaining candidates (Scheme 2). If the carboxylate of Asp-103 acts as the nucleophile, the intermediate will be a mixed anhydride species (Scheme 3A). The breakdown of the anhydride intermediate (k_3, the rate-determining step) should be accelerated by addition of exogenous nucleophiles such as hydroxylamine and methoxylamine. Also, either the product or the Asp-103 side chain of the enzyme should be covalently modified by the corresponding nucleophiles (Scheme 3A). If the enzyme is modified at Asp-103, its activity is expected to be adversely affected. However, if Zn1 hydroxide acts as the nucleophile, the intermediate will be a species attached to the enzyme through a Zn1−acyl linkage. The breakdown of this intermediate may also be accelerated by hydroxylamine and methoxylamine because they can displace the intermediate from the dinuclear Zn(II) center by ligand exchange (*48*), but the ligands must not bind the resting enzyme tightly or inhibition will result (Scheme 3B).

Initial results which showed that k_{cat} was accelerated by inclusion of exogenous nucleophiles were suggestive of a mixed anhydride intermediate, as was the low activity of a D103A mutant.[2] The acceleration effect could be assigned specifically to an increased rate of intermediate decay (k_3) by Fitsim and Kinsim simulations. Upon closer inspection, however, the observations that neither the product nor the enzyme side chain was modified and that enzyme activity was not affected after multiple turnovers in the presence of hydroxylamine and methoxylamine clearly do not favor the pathway via an anhydride intermediate. It is also unlikely that the enzyme is initially modified by attack of an exogenous nucleophile and the resulting adduct hydrolyzed to reform the active enzyme. The nucleophile−enzyme adduct would have to be exceedingly unstable and hydrolyze at a rate near that of the normal β-lactam substrate because the rate constant for the rate-limiting step (k_3) is near that of the steady-state turnover rate (k_{cat}). These results are more consistent with the proposal of a Zn1 hydroxide as the nucleophile and the observed intermediate as a novel anionic species bound to the enzyme through a Zn−acyl linkage (Scheme 3B). The exogenous nucleophiles accelerate the decay of EI, but do not bind tightly to the resting enzyme. Other dinuclear zinc enzymes have also been shown to change anion affinity throughout the reaction coordinate; fluoride inactivates the aminopeptidase from *Aeromonas proteolytica* only after substrate binding (*49*).

Why an Anionic Intermediate? Among the three metallo-β-lactamases whose structures are well characterized, the enzymes from *B. fragilis* and *S. maltophilia* have two tightly bound Zn(II) ions at their active site (*21*−*23*) while the *B. cereus* enzyme has one high- and one low-affinity Zn(II) binding site (*24*). Mechanistic studies of the *B. cereus* metallo-β-lactamase with only the high-affinity Zn(II)-binding site occupied suggested that hydrolysis proceeds via a dianionic tetrahedral intermediate formed by the nucleophilic attack on the β-lactam carbonyl by a Zn hydroxide (*34*, *35*). When nitrocefin was used as substrate for the *B. cereus* enzyme, the only spectral intermediate observed (under cryoenzymological conditions) had a visible absorbance band resembling that of the substrate but slightly red-shifted (to 440 nm), indicating that it is a nitrocefin-like, tetrahedral intermediate (*32*). There is no evidence of any kind to support a C−N bond cleaved intermediate in the catalytic cycle of the mono Zn(II) enzymes. However, enzyme-bound intermediates with almost identical red-shifted spectral features were observed during nitrocefin hydrolysis catalyzed by the dinuclear Zn(II)-containing *B. fragilis* (*39*) and *S. maltophilia* enzymes (*45*), suggesting that the second Zn(II) ion may play a very important role in the formation and stabilization of the anionic intermediate. Several models

[2] Z. Wang and S. J. Benkovic, unpublished results.

for substrate binding to the dinuclear Zn(II) active sites of metallo-β-lactamases have been generated on the basis of the three-dimensional structures (*28*−*31*). In all the models, Zn1 forms part of the oxyanion hole to polarize the carbonyl group of the β-lactam ring of the substrate. Nonenzymatic metal ion-catalyzed hydrolysis of β-lactams has been proposed to proceed through coordination of the metal ion to the lactam nitrogen (*50*). Zn2 is in close proximity to the β-lactam nitrogen of the substrate in the models, suggesting that it may very well interact with this nitrogen directly in the Michaelis complex to help position the substrate for the proper nucleophilic attack, to further polarize the amide bond, and to stabilize the negatively charged nitrogen of the leaving group during turnover. In addition, the apical water ligand of Zn2 may be displaced when substrate is bound. Therefore, it is likely that the strong electrostatic interaction between the negative charge of the intermediate and Zn2 and the lack of a well-positioned proton source prevents the negatively charged nitrogen from being protonated during C−N bond fission. Indeed, there are no general acid groups with kinetically significant pK_a values between 5.25 and 10.0 in the *B. fragilis* metallo-β-lactamase active site to donate a proton (*22*). It is interesting to note that this mechanism, metal ion stabilization of an anionic amine leaving group, had been anticipated by Page and co-workers in their studies of nonenzymatic metal ion-catalyzed hydrolysis and aminolysis of β-lactams (*50*, *51*).

Evidence for the strong electrostatic interaction between the dinuclear Zn(II) center and the negatively charged intermediate was obtained when a number of exogenous zinc ligands were used in the study presented here. Like hydroxylamine and methoxylamine, a variety of anions also accelerated the *B. fragilis* metallo-β-lactamase-catalyzed nitrocefin hydrolysis. As anions are usually better Zn(II) ligands than water, they increase the hydrolysis rate by weakening the electrostatic interaction in the enzyme-bound intermediate through ligand replacement (*48*). As with other dinuclear metalloproteins, the affinity of exogenous ligands for the metal center may be increased by binding of the substrate (*49*). Fluoride, acetate, fluoroacetate, and azide do not bind tightly to the free enzyme; any of these anions bound to the Zn(II) center after the breakdown of the enzyme-bound intermediate will be replaced immediately by water molecules from bulk solvent to regenerate the fully active enzyme. However, interaction of anions with the dinuclear center can be demonstrated through the use of a very good Zn(II) ligand, cyanate, which can bind more tightly to the dinuclear Zn(II) center of the enzyme. Low concentrations of cyanate increase the steady-state rates of the enzyme-catalyzed nitrocefin hydrolysis as weaker Zn(II) ligands do. High concentrations of cyanate can initially increase enzyme activity, but eventually inactivate the enzyme by ligating to the metal center, as observed with the dicobalt-substituted lactamase (Figure 5). There are several possible cyanate binding sites in the dinuclear Zn(II) center (Scheme 2). It can replace either the water molecule, the Zn1 hydroxide, or both; it can also become a fifth ligand to Zn1. The interaction of the *B. fragilis* metallo-β-lactamase with cyanate can be described kinetically by Scheme 4. However, the exact manner in which cyanate binds to the enzyme remains unclear.

Besides the dinuclear Zn(II) center, other parts of the substrate binding pocket and the surrounding areas may also contribute to the stability of the anionic intermediate. The hydrophobic pocket formed by the side chains of Ala-44, Ile-46, Val-52, and Ile-72 of the *B. fragilis* metallo-β-lactamase can accommodate the (2-thienylacetyl)amino substituent in nitrocefin very well (*29*). There is also a flexible loop, the so-called flap, formed by residues 45−51 near the substrate binding site (*29*). It was demonstrated that after the binding of a biphenyl tetrazole inhibitor to Zn2, residues in the flap provided hydrophobic side chains for interacting with the inhibitor, thus immobilizing the flap (*52*). This situation may occur after substrate binding; immobilization of the flap may protect the intermediate by shielding it from bulk solvent. This change, of course, will prolong the lifetime of the intermediate. Indeed, when three residues, 49−51, were deleted from the flap, no spectral intermediate was observed in nitrocefin hydrolysis by the mutant enzyme.[3]

In addition, the highly conjugated π-orbitals of the 2,4-dinitrostyryl group, the carboxylate substituent, and the double bond of the dihydrothiazine ring (Scheme 1A) delocalize the electrons, thus stabilizing the negatively charged intermediate. The accumulation of an enzyme-bound intermediate with a marked λ_{max} red shift from those of both the substrate and product (>110 nm) was also observed during the *B. fragilis* metallo-β-lactamase-catalyzed hydrolysis of another cephalosporin with highly conjugated substituents at the 3-position of the dihydrothiazine ring, BRL-54147AB-A (*53*) (see the Supporting Information). For substrates without a large conjugated π-system, it is very difficult to test this notion because of the lack of chromophores that exhibit distinct spectra, yet are not masked by the protein absorbance bands in the UV region. However, results from model studies of amide hydrolysis suggest that reduction of the leaving group amine basicity can destabilize N-protonated forms and facilitate expulsion of the leaving nitrogen without prior protonation (*54*). The fact that this intermediate is observed with the dizinc *B. fragilis* lactamase, but not with the monozinc *B. cereus* lactamase, suggests that the second zinc may provide this extra stabilization.

Proposed Mechanism. On the basis of the observations reported here and in our previous work, a mechanism of action of the *B. fragilis* metallo-β-lactamase is proposed (Scheme 5). In this scheme, the nucleophilic Zn1 hydroxide is preformed with a pK_a value of less than 5.25. Together with the conserved Asn-193, Zn1 also serves as the oxyanion hole to polarize the carbonyl group of the β-lactam ring of the substrate. The substrate carboxylate group, which is a necessity for binding all good substrates (*55*), forms a salt bridge either with Lys-184 or with Zn2 (not shown). The β-lactam nitrogen interacts with Zn2 and displaces the apical water molecule upon formation of the Michaelis complex. Zn1 hydroxide acts as the nucleophile which attacks the carbonyl group of the substrate. Cleavage of the C−N bond results in a negatively charged nitrogen leaving group which is stabilized by Zn2 through strong electrostatic interaction. Hydrolysis of β-lactams usually requires general acid protonation of the leaving group (*56*). However, in this instance, Zn2 substitutes for a proton, acting as a superacid. Product formation occurs upon the breakdown of the intermediate

[3] W. Fast, Z. Wang, and S. J. Benkovic, unpublished results.

Scheme 5: Proposed Mechanism of *B. fragilis* Metallo-β-lactamase Catalysis

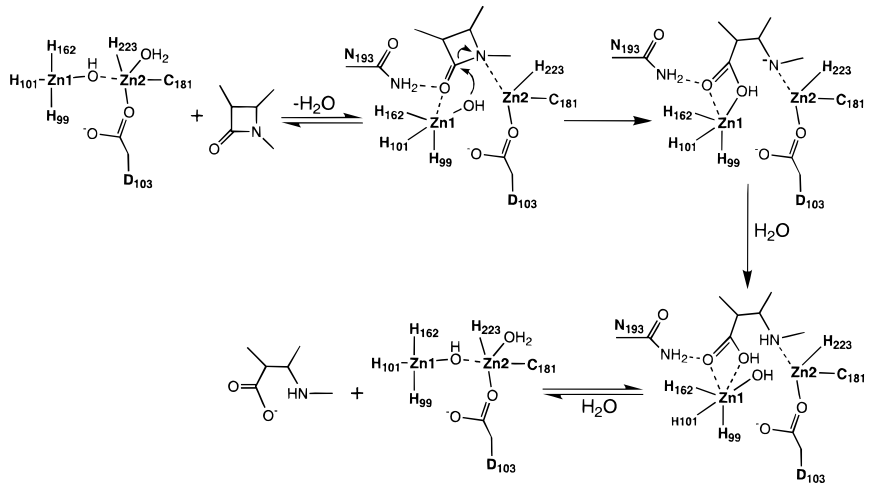

by protonation of the negatively charged nitrogen and ligand exchange at Zn1 of the acyl group of the intermediate with a water molecule from bulk solvent. The enzyme active site is then regenerated and ready for the next turnover. The role of Asp-103 in monozinc β-lactamase from *B. cereus* is thought to assist in formation of a dianionic tetrahedral intermediate and shuttle a proton to the leaving lactam nitrogen (*34*). In the dizinc β-lactamase of *B. fragilis*, general acid catalysis is not invoked, but Asp-103 may play a critical role in orienting Zn2 and the nucleophilic hydroxide, and in providing charge balance and corresponding attenuation of the Zn site electrophilicity. The mechanism of action of other group 3a metallo-β-lactamases, including the one from *S. maltophilia* and the enzyme from *B. cereus* when both Zn(II)-binding sites are occupied, may also follow the same pathway. However, the subtle differences in their active site structures may fine-tune each step in the pathway to achieve their distinct characteristics.

Earlier studies have reported that addition of a second zinc to a monozinc β-lactamase only increases the saturation hydrolysis rates from 80 to 100% of V_{max} (*22*, *24*). While this 1.25-fold increase in rate due to the addition of a second zinc is modest, it is also misleading as the two rates may represent different chemical steps. If the rates of C−N bond cleavage, rate-limiting in the *B. cereus* enzyme (*34*) [nitrocefin $k_{cat} = 45\ s^{-1}$ (*17*)] and assigned as k_2 ($3700\ s^{-1}$) in *B. fragilis*, are compared directly, a much different conclusion is reached which suggests that addition of the second zinc may increase the C−N cleavage rate by more than 80-fold. The full rate enhancement, however, is masked in k_{cat} by a change in the rate-limiting step. If the proposal that the monozinc β-lactamases are historical precursors to the dizinc β-lactamases is correct, then the appearance of a second zinc binding site represents an evolution of the catalytic mechanism for overcoming the kinetic barrier of C−N bond cleavage. This analysis carries an implicit threat; the fact that we can easily accelerate the new rate-limiting step, k_3, by addition of simple anions suggests that further catalytic improvements through evolution cannot be far off. The problem, however, with comparing β-lactamases from *B. cereus* and *B. fragilis* is their considerable sequence difference (66%) (*29*). We are currently studying the differences in rates for individual catalytic steps when a common protein scaffold is reconstituted with either 1 or 2 equiv of zinc.

With the exception of the unique anionic intermediate, this two-metal ion enzyme mechanism is similar to those proposed for other dinuclear hydrolases, such as aminopeptidases, phosphotriesterases, ureases, some restriction endonucleases, ribozymes, etc. (*57*, *58*). The utility of a dinuclear metal ion-containing active site ensures that one metal ion serves as a counterpart to the oxyanion hole and provides a metal hydroxide as a nucleophile while the other helps to position the substrate for proper nucleophilic attack, to further polarize the labile bond, and to stabilize the negative charge developed on the leaving group. The first metal ion is absolutely required for enzymatic activity; the addition of the second metal ion increases the enzyme efficiency. This may be why dinuclear hydrolases usually have higher catalytic efficiencies than mononuclear enzymes. Nucleophiles and anions may act as ligands to the metal ions, thus transiently destabilizing the intermediate by interrupting the electrostatic interaction between the metal ion and the leaving group through ligand exchange. If the nucleophile or anion in question does not bind to the active site of the resting enzyme tightly, it should accelerate the formation of the product as seen in this work. The rate-limiting decay of metal-bound intermediates may not be unique to the dinuclear β-lactamases. For example, acceleration of the dinuclear Zn(II)-containing leucine aminopeptidase-catalyzed leucine-*p*-nitroanilide hydrolysis by anions such as fluoride and azide was also reported (*59*).

ACKNOWLEDGMENT

We are grateful to Dr. Mark Wall for his help in the deprotonation studies. We also thank Dr. Beth A. Rasmussen at American Cyanamid Co. for the original *B. fragilis* metallo-β-lactamase (*CcrA*) clone, Dr. David J. Payne at SmithKline Beecham Pharmaceuticals for providing BRL-54147AB-A, and Dr. A. Daniel Jones at the Pennsylvania State University Mass Spectrometry Center for helping in the mass spectrometric analysis.

SUPPORTING INFORMATION AVAILABLE

Structures and UV−vis spectra of BRL-54147AB-A and its hydrolyzed product and spectral changes during the *B. fragilis* metallo-β-lactamase-catalyzed BRL-54147AB-A hydrolysis at pH 7.0 and 25 °C. This material is available free of charge via the Internet at http://pubs.acs.org.

REFERENCES

1. Philippon, A., Dusart, J., Joris, B., and Frère, J.-M. (1998) *Cell. Mol. Life Sci. 54*, 341−346.
2. Neu, H. C. (1992) *Science 257*, 1064−1073.
3. Davies, J. (1994) *Science 264*, 375−382.
4. Ambler, R. P. (1980) *Philos. Trans. R. Soc. London B289*, 321−331.
5. Bush, K., Jacoby, G. A., and Medeiros, A. A. (1995) *Antimicrob. Agents Chemother. 39*, 1211−1233.
6. Payne, D. J. (1993) *J. Med. Microbiol. 39*, 93−99.
7. Rasmussen, B. A., and Bush, K. (1997) *Antimicrob. Agents Chemother. 41*, 223−232.
8. Rossolini, G. M., Walsh, T. R., and Amicosante, G. (1996) *Microb. Drug Resist. (Larchmont, N.Y.) 2*, 245−252.
9. Bandoh, K., Watanabe, K., Muto, Y., Tanka, Y., Kato, N., and Uneo, K. (1992) *J. Antibiot. (Tokyo) 45*, 542−547.
10. Rossolini, G. M., Franceschin, N., Riccio, M. L., Mercuri, P. S., Perilli, M., Galleni, M., Frère, J.-M., and Amicosante, G. (1998) *Biochem. J. 332*, 145−152.
11. Senda, K., Arakawa, Y., Ichiyama, S., Nakashima, K., Ito, H., Ohsuka, S., Shimokata, K., Kato, N., and Ohta, M. (1996) *J. Clin. Microbiol. 34*, 2909−2913.
12. Watanbe, M., Iyobe, S., Inoue, M., and Mitshuashi, S. (1991) *Antimicrob. Agents Chemother. 35*, 147−151.
13. Ito, H., Arakawa, Y., Ohsuka, S., Wacharotayankun, R., Kato, N., and Ohta, M. (1995) *Antimicrob. Agents Chemother. 29*, 824−829.
14. Massova, I., and Mobashery, S. (1998) *Antimicrob. Agents Chemother. 42*, 1−17.
15. Osano, E., Arkawa, Y., Wacharotayankun, R., Ohta, M., Horii, T., Ito, H., Yoshimura, F., and Kato, N. (1994) *Antimicrob. Agents Chemother. 38*, 71−78.
16. Yang, Y., Rasmussen, B. A., and Bush, K. (1992) *Antimicrob. Agents Chemother. 36*, 1155−1157.
17. Felici, A., Amicosante, G., Oratore, A., Strom, R., Ledent, P., Joris, B., and Frère, J.-M. (1993) *Biochem. J. 291*, 151−155.
18. Felici, A., and Amicosante, G. (1995) *Antimicrob. Agents Chemother. 39*, 192−199.
19. Walsh, T. R., Gamblin, S., Emery, D. C., MacGowan, A. P., and Bennett, P. M. (1996*) J. Antimicrob. Chemother. 37*, 423−431.
20. Fujii, T., Sato, K., Miyata, K., Inoue, M., and Mitsuhashi, S. (1986) *Antimicrob. Agents Chemother. 29*, 925−926.
21. Crowder, M. W., Wang, Z., Frankilin, S. L., Zovinka, E. P., and Benkovic, S. J. (1996) *Biochemistry 35*, 12126−12132.
22. Wang, Z., and Benkovic, S. J. (1998) *J. Biol. Chem. 273*, 22402−22408.
23. Crowder, M. W., Walsh, T. R., Banovic, L., Pettit, M., and Spencer, J. (1998) *Antimicrob. Agents Chemother. 42*, 921−926.
24. Orellano, E. G., Girardini, J. E., Cricco, J. A., Ceccarelli, E. A., and Vila, A. J. (1998) *Biochemistry 37*, 10173−10180.
25. Valladares, M. H., Felici, A., Weber, G., Adolph, H. W., Zeppezauer, M., Rossolini, G. M., Amicosante, G., Frère, J.-M., and Galleni, M. (1997) *Biochemistry 36*, 11534−11541.
26. Carfi, A., Pares, S., Duee, E., Galleni, M., Duez, C., Frère, J.-M., and Dideberg, O. (1995) *EMBO J. 14*, 4914−4921.
27. Carfi, A., Duee, E., Galleni, M., Frère, J.-M., and Dideberg, O. (1998*) Acta Crystallogr. D54*, 313−323.
28. Fabiane, S. M., Sohi, M. K., Wan, T., Payne, D. J., Bateson, J. H., Mitchell, T., and Sutton, B. J. (1998) *Biochemistry 37*, 12404−12411.
29. Concha, N. O., Rasmussen, B. A., Bush, K., and Herzberg, O. (1996) *Structure 4*, 823−836.
30. Carfi, A., Soto, R.-P., Duee, E., Galleni, M., Frère, J.-M., and Dideberg, O. (1998*) Acta Crystallogr. D54*, 47−57.
31. Ullah, J. H., Walsh, T. R., Taylor, I. A., Emery, D. C., Verma, C. S., Gamblin, S. J., and Spencer, J. (1998) *J. Mol. Biol. 284*, 125−126.
32. Bicknell, R., and Waley, S. G. (1985) *Biochemistry 24*, 6876−6887.
33. Bicknell, R., Schäffer, A., Waley, S. G., and Auld, D. S. (1986) *Biochemistry 25*, 7208−7215.
34. Bounaga, S., Laws, A. P., Galleni, M., and Page, M. I. (1998) *Biochem. J. 331*, 703−771.
35. Page, M. I., and Laws, A. P. (1998) *Chem. Commun.*, 1609−1616.
36. Nord, C.-E., Olsson, B., and Dornbusch, K. (1978) *Scand. J. Infect. Dis. Suppl. 13*, 27−32.
37. Brook, I. (1989) *Ann. Clin. Lab. Sci. 19*, 360−376.
38. Rasmussen, B. A., Bush, K., and Tally, F. P. (1993) *Clin. Infect. Dis. 16*, 390−400.
39. Wang, Z., Fast, W., and Benkovic, S. J. (1998) *J. Am. Chem. Soc. 120*, 10788−10789.
40. Beechem, J. M. (1992) *Methods Enzymol. 210*, 37−53.
41. Barshop, B. A., Wrenn, R. F., and Frieden, C. (1983) *Anal. Biochem. 130*, 134−145.
42. Dang, Q., and Frieden, C. (1997) *Trends Biochem. Sci. 22*, 317.
43. O'Callaghan, C. H., Morris, A., Kirby, S. M., and Shingler, A. H. (1972) *Antimicrob. Agents Chemother. 1*, 283−288.
44. Cleland, W. W. (1977) *Adv. Enzymol. Relat. Areas Mol. Biol. 45*, 273−387.
45. McManus-Munoz, S., and Crowder, M. W. (1999) *Biochemistry 38*, 1547−1553.
46. Charney, E., and Bernhard, S. A. (1967) *J. Am. Chem. Soc. 89*, 2726−2733.
47. Barzaghi, M., Gamba, A., Morosi, G., and Simonetta, M. (1974) *J. Phys. Chem. 78*, 49−56.
48. Cotton, F. A., and Wilkinson, G. (1988) *Advanced Inorganic Chemistry*, 5th ed., pp 1285−1306, John Wiley & Sons, New York.
49. Chen, G., Edwards, T., D'souza, V. M., and Holz, R. C. (1997) *Biochemistry 36*, 4278−4286.
50. Gensmantel, N. P., Proctor, P., and Page, M. I. (1980) *J. Chem. Soc., Perkins Trans. 2*, 1725−1732.
51. Gensamantel, N. P., Gowling, E. W., and Page, M. I. (1978) *J. Chem. Soc., Perkins Trans. 2*, 335−342.
52. Toney, J. H., Fitzgerald, P. M. D., Grover-Sharma, N., Olson, S. H., May, W. J., Sundelof, J. G., Vanderwall, D. E., Cleary, K. A., Grant, S. K., Wu, J. K., Kozarich, J. W., Pompliano, D. L., and Hammond, G. G. (1998) *Chem. Biol. 5*, 185−196.
53. Burton, G., Fell, S. C. M., and Bateson, J. H. (1991) U.S. Patent 5,064,649.
54. Brown, R. S., Bennet, A. J., and Slebocka-Tilk, H. (1992) *Acc. Chem. Res. 25*, 481−488.
55. Laws, A. P., and Page, M. I. (1989) *J. Chem. Soc., Perkin Trans. 2*, 1577−1581.
56. Page, M. I. (1984) *Acc. Chem. Res. 17*, 144−151.
57. Sträter, N., Lipscomb, W. N., Klabunde, T., and Krebs, B. (1996) *Angew. Chem., Int. Ed. 35*, 2024−2055.
58. Wilcox, D. E. (1996*) Chem. Rev. 96*, 2435−2458.
59. Ludewig, M., Lasch, J., Kettmann, U., Frohne, M., and Hanson, H. (1971) *Enzymologia 41*, 60−67.

BI990356R